

UC Davis

UC Davis Previously Published Works

Title

Atrial natriuretic peptide down-regulates neutrophil recruitment on inflamed endothelium by reducing cell deformability and resistance to detachment force

Permalink

<https://escholarship.org/uc/item/24n5j2qk>

Journal

Biorheology, 52(5-6)

ISSN

0006-355X

Authors

Morikis, Vasilios A
Radecke, Chris
Jiang, Yanyan
[et al.](#)

Publication Date

2015

DOI

10.3233/bir-15067

Peer reviewed

1 **Atrial natriuretic peptide down-regulates neutrophil recruitment on inflamed endothelium**
2 **by reducing cell deformability and resistance to detachment force.**

3
4 Vasilios A. Morikis*¹, Chris Radecke¹, Yanyan Jiang¹, Volkmar Heinrich¹, Fitz-Roy Curry^{1,2},
5 Scott I. Simon¹

6 ¹Department of Biomedical Engineering, University of California, Davis USA 95616

7 ²Department of Physiology and Membrane Biology, School of Medicine, University of
8 California, Davis USA 95616

9

10

11

12

13

14

15 Text word count: 7,881

16 Abstract word count: 189

17 Number of figures and tables: 6

18 Number of references: 55

19 *Department of Biomedical Engineering
20 451 E. Health Sciences Drive
21 GBSF, Room 2303 University of California
22 Davis, CA 95616
23 vamorikis@ucdavis.edu
24 (530) 754-5739

1 **Abstract**

2

3 **BACKGROUND:** ~~In Japan,~~ Recombinant atrial natriuretic peptide (ANP) is administered in
4 patients with acute heart failure **in Japan** to improve renal function and hemodynamics, but its
5 anti-inflammatory effect on activated leukocytes may also contribute to its therapeutic efficacy

6

7 **OBJECTIVE:** Examine unconventional role of ANP in neutrophil adhesion to inflamed
8 endothelium.

9

10 **METHODS:** Human neutrophils were perfused over endothelial monolayers in a microfluidic
11 lab-chip assay. Cell rheology was assessed by micropipette aspiration to assess changes in
12 cortical tension and viscosity. Fluorescence microscopy was applied to measure adhesive contact
13 area and β_2 -integrin focal bond formation.

14

15 **RESULTS:** ANP inhibited neutrophil rolling and firm adhesion without influencing the
16 upregulation of cellular adhesion molecules on endothelium or **the regulation of** high affinity
17 CD18 and shedding of L-selectin during neutrophil activation. ~~Conversion~~ **Exposed to fluid**
18 **shear, to-shear-resistant** integrin mediated arrest was disrupted with ANP treatment, which
19 elicited formation of long tethers and diminished cell spreading and contact. This correlated with
20 **an** ~40% increase in neutrophil viscosity and a reduction in the adhesive footprint.

21

22 **CONCLUSIONS:** A decrease in cell deformation and ~~PMN-neutrophil~~ flattening with ANP
23 results in fewer integrin bond clusters, which translates to higher tensile forces and impaired
24 adhesion strengthening and cell detachment.

25

1 **1 Introduction**

2 Leukocyte recruitment is a necessary step in the innate immune response to infection and
3 inflammation and is crucial for wound healing [1]. The most common leukocyte in human
4 circulation are polymorphonuclear leukocytes, commonly denoted neutrophils (PMN). They
5 undergo a multi-step process of recruitment at vascular sites of infection and inflammation.
6 Inactivated or resting PMN circulate in the blood stream and a fraction are captured by tethering
7 through E-selectin (CD62E) and P-selectin (CD62P) upregulated on the endothelial surface,
8 which recognize leukocyte selectin (L-selectin or CD62L) and P-selectin glycoprotein ligand-1
9 (PSGL-1) that are constitutively expressed on the PMN surface [1]. PMN transition from selectin
10 mediated rolling to arrest can be activated by two distinct mechanisms: β_2 -integrins are
11 allosterically activated to a high affinity conformation through inside-out signaling following
12 ligation of G-protein-coupled receptors (GPCR), and through outside-in signaling via membrane
13 clustering of E-selectin ligands during cell rolling [2,3]. Both pathways lead to formation of
14 high-affinity β_2 -integrin bonding with intracellular adhesion molecule-1 (ICAM-1). Formation of
15 clusters of such bonds then triggers a flux of calcium that catalyzes F-actin polymerization,
16 which in turn facilitates PMN shape change to a polarized shape that orients the process of
17 migration through the endothelium towards sites of infection and inflammation [4,5]. This
18 inflammatory response of PMN can be deleterious under hyper-inflammatory conditions such as
19 tissue ischemia during acute myocardial infarction, which elicits a rapid increase in circulating
20 numbers and unchecked recruitment [6-7]. Therapeutic use of antagonists to the selectins,
21 integrins, and super-Ig adhesion molecules upregulated on leukocytes and endothelium has
22 shown mixed results and there are currently few antibodies or small molecules available for
23 clinical use [8-9]. This has motivated the discovery of biological strategies for ameliorating the
24 chronic over recruitment of PMN to inflamed endothelium [8].

25 The discovery of atrial natriuretic peptide (ANP) has provided evidence that the heart
26 functions not only as a pump, but also as a secretory organ that can regulate blood pressure, fluid
27 volume, and electrolyte balance. ANP is released by muscle cells in the atria of the heart and
28 binds guanylyl cyclase-A (GC-A) leading to biological actions through a cGMP-dependent
29 pathway [10]. ANP has long been established as a regulator of plasma volume by acting on renal
30 water and sodium excretion, as well as modulating vasodilation and the distribution of plasma
31 proteins between blood and body tissue. Recent studies indicate that ANP expression is increased
32 in infarcted regions of the left ventricle implying its potential importance in local regulation
33 during myocardial infarction (MI) [11]. Recombinant ANP (carperitide) was approved for
34 treatment of acute heart failure in Japan in 1995. However, the FDA in the USA has yet to
35 approve it for treatment and the majority of studies regarding ANP are performed in Japan in
36 patients with decompensated heart failure [12]. One large observational study was conducted on
37 3,777 patients with acute heart failure, in which carperitide was given at an average dosage of 85
38 ng/kg/min for 65 hours, resulting in a clinical improvement in 82% of patients [13]. While the
39 action of carperitide has been attributed mainly to its renal and vasodilatory actions, ANP's

1 effects on cell rheology and endothelial permeability have motivated ~~studies~~~~increased efforts~~ to
2 understand the actions of ANP in attenuation of the inflammatory recruitment of leukocytes that
3 are reported to reduce left ventricular remodeling following MI [14].

4 The role of ANP as a modulator of the innate immune response to tissue injury is not well
5 defined in part because different mechanisms of action of ANP have been ascribed to a variety of
6 mechanisms in a diversity of cell types involved in the innate immune response, including
7 endothelium, PMNs, mast cells, and macrophages [15]. For example in LPS-induced acute lung
8 injury in mice, ANP was reported to reduce E-selectin upregulation on pulmonary artery
9 endothelial cells and the release of tumor necrosis factor-alpha (TNF- α) [16]. There are also
10 reports of ANP acting on cytoskeletal components including regulation of the actin capping
11 protein HSP27 that promotes conversion of G- to F-actin [17] and contraction of microtubules
12 via Rho dependent pathways [18]. ANP has also been shown to inhibit lipopolysaccharide
13 (LPS)-induced Nitric Oxide release in macrophages by binding to NPR-A receptors to increase
14 cGMP [15]. An increase in cGMP can inactivate Nuclear Factor-kappa B and increase cytosolic
15 calcium in murine macrophages [17]. The effects of ANP on PMN function following activation
16 has been controversial, with reports of ANP acting to prime PMN for activation but also to
17 attenuate release of super oxide and matrix metalloproteins. [16, 19-21].

18 ANP primarily induces its biological effects through natriuretic peptide receptors (NPR) A
19 and C. NPR-A ~~has been shown to activate~~s particulate guanylate cyclase thereby increasing
20 guanosine 3',5'-cyclic monophosphate (cGMP) while NPR-C ~~has been shown to regulate~~
21 adenylate cyclase and membrane/lipid turnover by activation of specific phospholipases. Both
22 Human macrophages and THP-1 cells ~~have been previously shown to reportedly~~ express
23 natriuretic peptide receptors (NPR-A, -B, and -C) [22]. ~~Further, m~~Macrophages treated with
24 ANP ~~has been shown to~~ enhance reactive oxygen species (ROS) production primarily via
25 natriuretic peptide receptor-C (NPR-C). ~~In the case of endothelium, ANP's effects on~~
26 ~~endothelium has~~are largely ~~been~~ attributed to NPR-A, which is densely expressed in the
27 microvasculature. ANP ~~has been shown reported to is reported to~~ increase vascular permeability
28 under some conditions and to protect the ~~vascular barrier to leakage~~ under others by affecting
29 endothelial cAMP levels ~~depending on relative expression of~~via endothelial cell
30 phosphodiesterases 2A and 3A and the levels of cGMP ~~stimulation~~ [23].

31 The goal of the current study is to delve into the actions of ANP on PMN activation and
32 recruitment to inflamed endothelium. We report that ANP reduces PMN rolling, arrest, and
33 transendothelial migration through a mechanism independent of alterations in expression and
34 function of adhesion receptors on the endothelium and PMN. Cell rolling and the transition to
35 arrest is modulated by bulk cell deformation, microvillus deformability, and receptor-ligand
36 binding kinetics [24-26]. A remarkable observation is that capture of PMN via selectins, which
37 mediates tether formation and rolling, ~~did not~~ converted to shear resistant integrin dependent
38 arrest ~~with lower efficiency~~ in the presence of ANP. This was due to abrupt rupture of long
39 tethers that formed as shear was incrementally ramped. Rheological analysis of PMN

1 deformation using micropipette aspiration revealed that ANP enhances PMN viscosity and this
2 correlated in a dose dependent manner with diminished recruitment efficiency on inflamed
3 vasculature.

4 **2 Methods**

5 *2.1 Antibodies, small molecules, and other reagents*

6 Recombinant human ICAM-1-Fc, E-selectin-Fc, and CXCL8/IL-8 were purchased from
7 R&D Systems (Minneapolis, MN; Catalog No. 720-IC, 724-ES, and 208-IL respectively).
8 Protein A/G was purchased from Fischer Scientific (Pittsburgh, PA). BS3 crosslinker, Alexa
9 Fluor 488 Phalloidin and Vybrant DiI Cell-Labeling Solution was purchased from life
10 technologies (Grand Island, NY). Antibodies used in flow cytometry, FITC mouse anti-human
11 CD106 (VCAM-1), PE-Cy5 mouse anti-human CD62E (E-selectin), and PE-Cy5 mouse anti-
12 human CD54 (ICAM-1) were purchased from BD Biosciences (San Jose, CA) while Alexa Fluor
13 488 mouse anti-human CD11a/CD18 (mAb24, LFA-1), PE mouse anti-human CD162 (PSGL-1),
14 and PE-Cy5 mouse anti-human CD62L (L-selectin) were purchased from Biolegend (San Diego,
15 CA). Antibodies were used at a saturating concentration of 5 µg/mL or per manufacturer's
16 instruction. Human atrial natriuretic peptide (ANP) was purchased from BACHEM (Torrance,
17 CA). Normal human primary umbilical vein endothelial cells (HUVEC) were purchased from
18 ATCC (Manassas, VA). Recombinant human IL-1β was purchased from eBioscience (San
19 Diego, CA).

20 *2.2 Wound model in Lys-M-EGFP mice*

21 The Lys-M-**enhanced green fluorescent protein (EGFP)** stable mouse strain and the skin
22 wound model for non-invasive whole animal fluorescent imaging of EGFP neutrophils was
23 performed as previously described [27]. In brief, mice were anesthetized and hair was removed
24 with a mechanical shaver prior to a 6 mm in diameter full thickness wound was made using a
25 biopsy punch (Robbins Instruments, Chatham, NJ). The *in vivo* imaging of EGFP neutrophils
26 appearing on the flank of mice with skin wounds was performed using whole animal
27 fluorescence imaging system (Xenogen IVIS 100 system, Xenogen) as the neutrophils were
28 visualized using a GFP filter (excitation 445-490 nm and emission 515-575 nm). We have
29 previously measured the steady accumulation of EGFP labeled PMNs in the wound for an hour,
30 24 hours post wounding [27]. The rate of accumulation of PMN 24 hours post wounding was
31 stimulated over a period of 1 hour after adding thrombin (5 U/ml, Sigma-Aldrich) to the wound.
32 Direct perfusion of 50 ng/kg BW/min of ANP and its effect on the rate of accumulation of PMNs
33 (arbitrary fluorescence intensity/min, FI/min) was measured, as previously described [27].

34 *2.3 Neutrophil Isolation*

35 PMNs were isolated from freshly collected human blood from healthy donors consented
36 through an approved by the University of California, Davis institutional review board protocol.

1 Whole blood was layered over PMN separation media, Polymophoprep purchased from Axis
2 Shield formulations purchased from Cosmo Bio USA, as previously described (1). After
3 centrifugation PMN cells were extracted and washed with 4-(2-hydroxyethyl)-1-
4 piperazineethanesulfonic acid buffered salt solution. PMN were treated with ANP (0-100 nM)
5 for 30 minutes at room temperature under agitation prior to use.

6 *2.4 Flow Cytometry*

7 Flow cytometry was used to quantify the presence of VCAM-1, ICAM-1, and E-selectin
8 on HUVEC in the presence and absence of ANP. HUVEC monolayers were grown to high
9 confluence overnight according to ATCC supplied protocols. HUVEC monolayers were then
10 treated with 0.2 ng/mL of IL-1 β for 4 hours and incubated with ANP (0-100 nM) 30 minutes
11 prior to harvesting. Cells were harvested via 1 mM EDTA chelation and spun down. After
12 collection, suspended cells were incubated with FITC conjugated mouse anti-human CD54 and
13 PE-Cy5 conjugated mouse anti-human CD62E or PE-Cy5 conjugated mouse anti-human ICAM-
14 1. Flow cytometry was also used to quantify ANPs ability to activate PMNs in suspension and
15 alter actin polymerization. Whole blood was obtained by venipuncture and PMNs were
16 immediately isolated and treated with ANP (0-10 nM) for 30 minutes. Cells were then incubated
17 with Alexa Fluor 488 mouse anti-human mAb24 to label high affinity LFA-1, PE mouse anti-
18 human PSGL-1, and PE-Cy5 mouse anti-human L-selectin, or Alexa Fluor conjugated Phalloidin
19 with simultaneous fixing and permeabilization, with and without IL-8 stimulation. Data was
20 acquired by flow cytometry (BD FACScan) and quantified (FlowJo) as mean fluorescent
21 intensity and plotted as fold change compared to 0 nM ANP conditions. All experiments were
22 performed in triplicates.

23 *2.5 Adhesion Assays*

24 HUVECs were cultured onto 35 mm diameter, #1.5 glass coverslips over to tight
25 confluence as per supplied ATCC protocols. HUVEC monolayers were then treated with 0.2
26 ng/mL of IL-1 β for 4 hours and incubated with ANP (0-100 nM) 30 minutes prior to use.
27 Custom multi-channel microfluidic device were assembled on coverslips as previously described
28 [2,4-5] and isolated PMNs were perfused at a concentration of 1×10^6 cells/mL at a physiological
29 shear of 2 dynes/cm². For adhesion strengthening experiments 25 mm diameter, #1.5 glass
30 coverslips were piranha etched to remove organic molecules and to deposit hydroxyl group
31 molecules on the surface. The etched coverslips were submerged in Acetone with 1% 3-
32 aminopropyltriethoxysilane (APTES) to add aminosilane groups and recombinant human ICAM-
33 1-Fc along with E-selectin-Fc were absorbed at 5 μ g/mL concentration for 1 hour. Isolated
34 human PMNs at 10^6 cells/mL treated with ANP (0-100 nM) were allowed to settle over the
35 ICAM-1 + E-selectin substrate. Shear was then ramped at 30 second intervals from 0, 4, 10, 20,
36 to 40 dynes/cm², and the number of cells that remained adhered were measured over seven
37 separate fields of view along the centerline of the channel at each shear level. Cell arrest was

1 defined as a PMN that translated on the substrate less than 50% of a cell diameter ($\sim 4 \mu\text{m}$) in a
2 10 second interval

3 *2.6 Rheological Analyses*

4 Micropipettes with an evenly broken, cylindrical tip of the desired inner diameter ($\sim 2 \mu\text{m}$
5 for hemisphere aspiration and $\sim 4 \mu\text{m}$ for full aspirations) were made prior to experimentation, as
6 described previously (2). To ensure PMN quiescence while imaging 10% heat treated autologous
7 serum was added to the experimental buffer and coated the chamber and micropipettes. A small
8 volume of cell suspension at 1×10^6 cells/mL was introduced into the experimental chamber (~ 5
9 μL). Assuming cortical tension, γ , is uniform and isotropic Laplace's law can be used in terms of
10 aspiration pressure within the pipette to solve for cortical tension, σ .

$$\sigma = \frac{1 \Delta p R R_p}{2 R - R_p}$$

11 Where R is the radius of the spherical main cell body and R_p is the pipette radius (26). The
12 protrusion length at every pressure and radius of the cell is estimated assuming the volume of the
13 cell is kept constant. The radius of the outer portion of the cell was calculated by the following
14 geometrical equation:

$$R = (R_i^3 - \frac{3}{4} R_p^2 L_p + \frac{1}{4} R_p^3)^{\frac{1}{3}}$$

15 where R_i is the radius of the untouched cell and R_p is the radius of the pipette. Cell surface area
16 was then estimated by describing cell geometry in terms of spherical and cylindrical components
17 and tension was then computed using Laplace's equation. The cortical tension is obtained by
18 plotting the fractional increase in area expansion from 0 to 0.35 as PMN are aspirated to different
19 extents. Resting cortical tension was inferred from the data by fitting a straight line to the low-
20 pressure values and the y-intercept of the linear fit is a measure of the resting cortical tension. To
21 estimate the elastic constants of PMN recovery a derivative of the classical "cortical shell-liquid
22 core model" was implemented. The analysis provides an approximate analytical solution to the
23 equations of creeping flow of a Newtonian droplet with a moving, pre-stressed boundary [29-
24 32]. The model assumes a constant cortical tension and predicts the time dependent recovery,
25 measured as the ratio of cell length to width. Custom-written software interfaced with a joystick
26 allowed for three dimensional manipulation of the micropipettes in three dimensions and video
27 was recorded (30 frames per second) of the gentle aspiration of cells. For the full aspiration
28 experiments cells are slowly pulled entirely into the pipette and held there for 10 seconds prior to
29 being ejected back into the chamber. A Tran-Son-Tay model was used to study the time
30 dependence of the ratio of length/width of the recovering PMN resulting in an estimate of the
31 ratio between cortical tension and viscosity, σ/η [29,30].

32 *2.7 Quantitative Dynamic Footprinting*

1 An inverted TIRF research microscope (Nikon) equipped with a 60X numerical aperture
2 1.5 immersion TIRF objective and a motorized stage using a 543 solid state lasers as TIRF
3 excitation light sources and the appropriate filter set. A 120 W arc lamp was used to capture epi-
4 fluorescence images. Images were captured using a 16-bit digital complementary metal oxide
5 semiconductor (CMOS) camera (Andor ZYLA) connected to a PC (Dell) with NIS Elements
6 imaging software. Images were captured with 2x2 binning at a resolution of 1024 x 1024 at a rate
7 of 2 frames per seconds. An incidence angle of approximately $\theta = 70^\circ$ was used for all
8 **quantitative dynamic footprinting (qDF)** experiments. Isolated PMNS at 1×10^6 cells/mL were
9 stained with Vybrant membrane dye DiO and flown in to our custom microfluidic chip at 1
10 dyne/cm² along with high affinity LFA-1 antibody mAb24 slowly and allowed to adhere on an
11 ICAM-1 + E-selectin substrate. Shear was ramped incrementally from 2 to 20 dynes/cm² and cell
12 contact area was observed along with focal adhesion complexes of LFA-1.

13 *2.8 Data Analysis and Statistics*

14 Data are reported as mean \pm SEM. Multiple groups were compared using one-way
15 ANOVA with Tukey posttest. All analyses were carried out using GraphPad Prism 5.01 for
16 Windows (GraphPd Software, San Diego, CA).

17

1 3 Results

2 3.1 ANP down-regulates PMN recruitment on inflamed endothelium independent of changes cell 3 adhesion molecule function.

4 In a full thickness skin wound on the flank of a mouse, we measured the steady
5 accumulation of LysM-EGFP labeled PMN into the wound bed 24 hours following injury using
6 whole animal fluorescence imaging (Figure 1A)[27]. ANP (50ng/kg BW/min) perfused directly
7 into the wound bed for 60 min. elicited a small but not significant reduction compared to the
8 baseline number of PMN accumulating in the wound. The addition of thrombin directly to the
9 wound increased the rate of PMN influx by ~5-fold. Pretreatment with ANP for 30 min.
10 significantly reduced the PMN influx in response to thrombin stimulation. Given that ANP in the
11 circulation has a half-life of ~15 minutes [33], the average ANP concentration in the wound was
12 estimated to be 50-75nM. Under identical experimental conditions, a separate study by our group
13 revealed that ANP actually increased the vascular permeability of fluorescently labeled albumin
14 into the wound bed [34]. On the basis of these observations we investigated the mechanism by
15 which ANP could modulate PMN interaction with endothelium over a range of ANP
16 concentrations employing an *in vitro* model. HUVEC monolayers were inflamed with IL-1 β in
17 the presence of ANP to observe its capacity to alter the normal up-regulation of cellular adhesion
18 molecules ICAM-1, VCAM-1, and E-selectin (Figure 1C). Expression of cellular adhesion
19 molecules was quantified using fluorescently conjugated antibodies and detected by flow
20 cytometry on fixed and labeled HUVEC. A 300-fold increase in E-selectin, a 20-fold increase in
21 ICAM-1, and a 3-fold increase in VCAM-1 were measured in response to inflammatory
22 stimulation. No significant effect on the upregulation of the adhesion molecules was observed
23 over a physiological dose range of ANP after IL-1 β induced upregulation. Thus, ANP effectively
24 decreased PMN recruitment to inflamed endothelium independent of any affect on up-regulated
25 endothelial cell adhesion receptors.

26 To further understand how ANP may inhibit PMN accumulation, isolated PMNs were
27 pretreated with ANP and perfused over HUVEC monolayers and observed using phase contrast
28 light microscopy in a custom microfluidic flow channel [2,4-5]. PMN were sheared at 2
29 dynes/cm² in order to quantify the multistep process of cell capture and the transition from
30 rolling to arrest. Upon arrest, PMN undergo a rapid shape change defined as ~50% of cell area
31 converting to phase dark appearance. The frequency of PMN rolling and arrest at a low shear
32 stress of 2 dynes/cm² was significantly reduced by ~50% at 10 and 100 nM ANP compared to
33 controls (p<0.01) following pretreatment (Figure 2A). Of the PMN that achieved firm arrest,
34 ~75% underwent shape change and transendothelial migration (TEM), which was not inhibited
35 by ANP treatment (Figure 2A).

36 To elucidate ANP's effect on PMN adhesion strengthening following cell arrest
37 independent of its effect on the endothelium, PMN were perfused through the microfluidic flow
38 channel on a substrate of recombinant E-selectin and ICAM-1. This combination of endothelial

1 adhesion receptors supports E-selectin mediated slow rolling and CD18 activation and shear
2 resistant arrest [3,4]. To further examine the dose dependent action of ANP, shear was
3 incrementally ramped from 2 to 40 dynes/cm² and the fraction of PMN remaining attached to the
4 substrate was measured (Figure 2B). PMN treated with ANP demonstrated a significantly
5 diminished capacity to convert to shear resistant arrest. Control PMN formed short tethers upon
6 conversion to an arrested state, those treated with ANP consistently formed long tethers that
7 abruptly ruptured causing PMN to return to the flow field. A dose dependence was detected in
8 which half the PMN detached at a shear stress of 20-30 dynes/cm² at 1 nM ANP. At the higher
9 dose of 10 nM ANP, detachment of half the PMN was observed at 10-20 dynes/cm². At the high
10 dose of ANP, complete detachment was observed at 30 dynes/cm². During shear ramping from 2
11 dynes/cm² to 10 dynes/cm², the dynamics of tether formation was recorded for firmly adherent
12 PMN as shear was ramped from 2 dynes/cm² to 10 dynes/cm². To quantify deformation of PMN
13 sheared in the flow channel, the maximum tether length is plotted as a function of the dose of
14 ANP. This reveals a significant increase in tether length prior to detachment compared with
15 untreated control (Figure 2C). Taken together, the adhesion behavior of PMN indicates that cell
16 activation and changes in rheology may be affected by treatment with ANP.

17 To evaluate the effect of ANP on the signaling of PMN activation in response to
18 stimulation with IL-8, conversion of CD18 to high affinity was detected using the activation
19 reporter antibody mAb24 and shedding of L-selectin was quantified as a loss of antibody binding
20 (Figure 2D). In response to stimulation, PMN registered a 10 fold upregulation in the high
21 affinity state of β_2 -integrin and shed L-selectin to levels equivalent to binding of IgG control
22 antibody. The presence of ANP at 1 or 10 nM had no effect on these measures of PMN
23 activation compared to untreated conditions. To determine if ANP altered cytoskeletal activation
24 total F-actin expression was measured with Phalloidin in PMN stimulated with IL-8 in
25 suspension (Supplementary Figure 2). No significant change in these measures of PMN
26 activation were observed between PMN stimulated in presence of vehicle control versus ANP
27 treatments.

28 *3.2 ANP increases PMN viscosity without changing cortical tension*

29 To quantify the viscoelastic properties of PMN the ratio between cortical tension (σ) and
30 viscosity (η) was examined by direct manipulation in micropipette studies. Cell relaxation from
31 a deformed cylinder back to a spherical state following aspiration into a micropipette and release,
32 was measured in isolated unstimulated PMN. Cells were subjected to deformation and held in the
33 micropipette for ten seconds and then gently expelled into the chamber (Figure 3A). Cell
34 recovery back to a spherical shape as a function of time required ~70 seconds for untreated cells
35 and ~120 seconds in the presence of 10 nM ANP. An estimate of the ratio between cortical
36 tension and viscosity (σ/η) is given as a fitting parameter in the “cortical shell-liquid core” model
37 of cellular mechanics (see Methods) as depicted by the histograms that compares untreated with
38 10 nM ANP treated (Figure 3C). ANP resulted in a 40% decrease in the ratio of cortical
39 tension/viscosity ($\sigma/\eta_{\text{untreated}} = 0.117$ and $\sigma/\eta_{\text{ANP}} = 0.070$).

1 Next we measured resting cortical tension by partially aspirating PMN at defined
2 micropipette pressure and measured the projection length (L_p) as pressure was increased in until
3 the projection length remained constant (Figure 3D). Using the analysis described in methods
4 resting cortical tension was found to be 0.021 ± 0.003 nN/m for untreated cells and 0.023 ± 0.007
5 nN/m for 10 nM ANP treatments. No significant difference in the magnitude of the resting
6 cortical tension was found between controls versus ANP treatment. Measured values of σ and
7 σ/η in PMNs were not significantly different from previous reports of human granulocytes
8 (Table 1). Our value of cytoplasmic viscosity for untreated cells was ~ 179 Pa·s, which is in close
9 agreement with previous observations (25-28,32-34), whereas those treated with ANP were
10 nearly 1-fold higher at a value of ~ 324 Pa·s. We conclude that ANP elicited a significant
11 increase in cytosolic viscosity even in the absence of PMN activation.

12 *3.3 ANP decreases PMN deformability and adhesive footprint on ICAM-1 under shear flow*

13 PMN were labeled with the membrane dye Vybrant DiO and sheared in microfluidic
14 channels on an E-selectin and ICAM-1 substrate at a shear stress of 1 dynes/cm² to promote cell
15 rolling and arrest. Shear was then incremented and the change in membrane contact area of
16 adhesive PMN was determined over time using TIRF microscopy. As depicted in the
17 fluorescence images, PMN establish an initial area of contact and steadily become elongated in
18 the direction of shear flow (Figure 4 A). PMN formed a smaller area of contact in the presence of
19 ANP and did not exhibit an increase in area over time at constant shear stress (Figure 4B). As
20 shear stress was incremented, untreated PMN nearly tripled the area of adhesive contact, while
21 for ANP treated cells the area remained constant (Figure 4C). Since it was observed that
22 exposure to 10 nM ANP elicited premature detachment in the majority of PMN as shear was
23 ramped to 10 dynes/cm², we examined the formation of high affinity CD18 bonds to ICAM-1 in
24 untreated and ANP treated adherent PMN (Figure 4D). Consistent with expression of high
25 affinity CD18 in stimulated suspensions of PMN, the overall level of CD18 in contact with
26 ICAM-1 following rolling to arrest was equivalent for untreated and ANP treated PMN.
27 However, formation of focal clusters of CD18 bonds was significantly diminished in presence of
28 ANP as compared with untreated PMN. Formation of high affinity CD18 bond clusters is
29 required for PMN adhesion strengthening following arrest and spreading on the substrate [37].
30 We conclude that ANP treatment disrupts the capacity of attached PMN to deform and spread on
31 the substrate resulting in a smaller adhesive footprint containing fewer CD18 bond clusters that
32 prematurely fail compared with normal adhesion strengthening.

33

1 4 Discussion

2 ANP is produced by the heart during atrial distension and has been shown to be a modulator of
3 the innate immune response, yet detailed studies of ANP's anti-inflammatory mechanisms
4 relevant to reduction of PMN interaction with the endothelial wall have not been investigated
5 [15, 38,39]. ANP has previously been used to treat patients with heart failure due to its diuretic
6 and vasodilatory actions [13,14]. However, anti-inflammatory effects, especially to reduced
7 PMN interaction with activated endothelium, have not been investigated. Directly imaging PMN
8 trafficking into a full thickness skin wound, we observed acute treatment with ANP exerted a
9 significant inhibitory effect on thrombin stimulated PMN recruitment. **Thrombin activates**
10 **Proteinase-activated receptors (PAR) 1 and 4 to inducing a proinflammatory phenotype through**
11 **upregulation of VCAM-1, ICAM-1, and E-selectin endothelium-dependent relaxation, with**
12 **minimal effect on smooth muscle. Thrombin induces an increased nitric oxide production along**
13 **with an elevation in calcium by inhibiting phosphorylation of eNOS at Ser1177 dependent on the**
14 **RhoA-Rho kinase pathway. Thrombin has also been shown to induce a proinflammatory**
15 **phenotype through upregulation of VCAM-1, ICAM-1, and E-selectin [40,41].** ~~We assessed the~~
16 ~~mechanism using an in-vitro assay in which PMN were sheared over HUVEC and discovered~~
17 ~~that ANP down-regulated their recruitment to inflamed endothelium by ~40% primarily through~~
18 ~~antagonizing the transition to shear resistant integrin ICAM-1 mediated arrest.~~ **Thrombin**
19 **stimulated adhesion is different from chemokine stimulated adhesion (such as fMLP and IL-8)**
20 **signaling that occurs primarily in PMN. A classical signaling pathway triggered by GPCR is the**
21 **biphasic Calcium-signal. The first phase of which is mediated by phospholipase C β which that**
22 **leads to generation of IP₃ and release of calcium from intracellular stores. Activation of**
23 **phosphatidylinositol P₃ (PIP₃) has also been implicated in GPCR stimulation via Src-Family**
24 **kinases. The TNF-receptor family can also signal PMN activation and prime subsequent**
25 **response to additional stimuli by recruiting adaptor proteins (TNFR1 and TNFR2, both present**
26 **on PMN) [42].** ~~We assessed the mechanism using an in-vitro assay in which PMN were sheared~~
27 ~~over HUVEC and discovered that ANP down-regulated their recruitment to inflamed~~
28 ~~endothelium by ~40% primarily through antagonizing the transition to shear resistant integrin-~~
29 ~~ICAM-1 mediated arrest.~~ ~~By interrogating PMN and HUVEC capacity to upregulate cellular~~
30 ~~adhesion molecules in response to inflammatory stimuli in the presence of ANP, we determined~~
31 ~~that~~ **It is noteworthy that** diminished recruitment occurred irrespective from changes in adhesion
32 molecule expression and function **on HUVEC**. Measurement of PMN rheology revealed that
33 treatment with ANP resulted in an increase in PMN cytoplasmic viscosity within minutes, while
34 the subsurface membrane cortical tension remained constant. Single cell image analysis of
35 adherent PMN deforming under shear stress revealed an increase in adhesive contact area and the
36 formation of membrane tethers, which was altered by ANP treatment. We conclude that ANP
37 effectively limits PMN recruitment to sites of inflammation by altering the normal response
38 characterized by an increase in the area of adhesive contact as cells spread and polarize on the
39 substrate. ANP nearly doubled PMN cytoplasmic viscosity and this corresponded to
40 significantly smaller adhesive contact and diminished formation of durable integrin bond

1 clusters. These observations correlated with a dose dependent increase in PMN detachment at
2 relatively low levels of shear stress.

3 Previous studies on the relationship between wall shear stress and leukocyte deformation during
4 rolling and arrest have shown that rolling velocity and frequency of arrest is invariant as shear
5 stress is incremented. This is due to the greater deformation of PMN that occurs as
6 hydrodynamic drag force is increased, which translates to increased contact area as depicted in
7 the schematic of Figure 5. As PMN spread there is more efficient conversion to cell arrest due to
8 an increase in integrin bond formation [43]. Over the duration of rolling to arrest, PMN transition
9 from an initially spherical state to a more flattened and elongated geometry that is attributed to
10 its viscoelastic properties [44]. An estimate of the extent of deformation can be gleaned from
11 application of a continuum model based upon measured material properties of the PMN under
12 resting and activated conditions [45,46]. Dembo et. al. derived a so called “tape-peeling” model
13 to examine the dynamics of the area of adhesive contact. This model proposed the cell be divided
14 into three regions; the macroscopic region where hydrodynamic shear forces predominate, the
15 microscopic region where receptor-ligand binding is initiated and receptor density is low, and the
16 adhesion layer where receptor density increases and bond formation occurs (Figure 5). During
17 cell rolling to arrest, shear forces are transmitted from the cell body to the substrate through
18 membrane tension and cell body forces. Cell deformation is critical in resisting the
19 hydrodynamic drag that acts on rolling PMN. For example, the magnitude of shear forces acting
20 on PMN positively correlates with the ratio of the height of the cell to vessel diameter [47]. A
21 concomitant effect of cell deformation and membrane spreading is a decrease in the angle (θ_b) at
22 which the resultant drag force acts on the bonds. An increase in adhesion contact area is
23 associated with increased bond formation, effectively countering the resultant shear force (F_s)
24 that acts to rupture nascent bonds (F_b) (Figure 5) [49,50]. The increase in cell viscosity induced
25 by ANP treatment was found to decrease the extent of deformation of PMN arrested on the
26 substrate, thus resulting in a smaller contact area at constant cell volume. This decrease in cell
27 deformation effectively reduced PMN capture, as well as their capacity to remain adherent (e.g.
28 adhesion strengthen) with increased shear stress. We hypothesize that ANP treated PMN exhibit
29 increased cytosolic viscosity and consequently do not flatten as much as untreated. This resulted
30 in a greater (θ_b) and higher tensile forces acting on membrane tethers and on integrin bond
31 clusters that form within smaller areas of adhesive contact. Tethers in ANP treated PMN were
32 twice as long and disruptive shear forces were distributed to fewer CD18 bond clusters resulting
33 in premature rupture at lower F_s compared with untreated cells.

34 The mechanism by which ANP increases PMN viscosity remains unknown and will
35 require additional inquiry. A potential molecular mechanism by which ANP increases the
36 cytoplasmic viscosity of PMN may act through a previously reported effector pathway for
37 thrombin attenuation and microtubule stabilization in endothelial cells [18]. According to Baldini
38 et. al. macrophages express natriuretic peptide receptors NPR-A, NPR-B, and NPR-C and ANP
39 treatment significantly decreases intracellular pH enhancing ROS production. Consequently

1 Although it is possible that ANP acts via these membrane receptors they act through in PMN, the
2 signaling pathway has yet to be reported in a similar manner. ANP has been shown signaling
3 through to stimulate Rac GTPase and its effector PAK1, which down-regulates GEF-H1
4 activation via phosphorylation at Ser⁸⁵⁵. One downstream consequence is reduced activation of
5 Rho-GTPases, which are key regulators of actin dynamics in vascular cells [51]. Additionally
6 ANP has been shown to stabilize microtubules, leading to its vasoprotective effects [18]. Rac2 is
7 another GTP-ase that plays a key role in PMN responses to inflammatory signaling, including
8 actin remodeling, chemotaxis, and superoxide production by NADPH oxidase [52,53]. Given the
9 observation that the cellular level of F-actin was not different between ANP and untreated PMN,
10 we hypothesize that ANP may alter the dynamic localization of F-actin, possibly by influencing
11 gelsolin dynamics through stimulation of Rac-GTPase [53,57]. Rac has been shown to promote
12 the dissociation of gelsolin from actin filaments in neutrophils thereby effecting F- to G-actin
13 ratio [58]. Thus, we speculate that ANP may disrupt the normal process by which gelsolin
14 regulates spatiotemporal actin dynamics and in turn affect cytosolic viscosity. This is consistent
15 with the finding of inefficient extravasation into the full thickness skin wound in presence of
16 ANP and the defect in conversion to shear resistant firm arrest and adhesion strengthening.
17 Further analysis of ANP's effect on PMN Rho-GTPases and local F-actin dynamics is necessary
18 to further elucidate its apparent effect on PMN viscosity.

19 In this study, we report that ANP significantly attenuates the thrombin augmented
20 inflammatory accumulation of PMN in skin wounds. We attribute this to ANP capacity to
21 increase cytosolic viscosity and provide a potential mechanism to explain the observation of
22 diminished PMN deformation and an inability to convert to shear resistant arrest. Further studies
23 on the relation between ANP and spatiotemporal control of F-actin dynamics and in turn the
24 effect on PMN viscosity could lead to its use as anti-inflammatory inside and outside of Japan.

25

5 References

- [1] Simon SI, Green CE. Molecular mechanics and dynamics of leukocyte recruitment during inflammation. *Annu Rev Biomed Eng.* 2005; 7: 151-185
- [2] Dixit N, Kim MH, Rossaint J, Yamayoshi I, Zarbock A, Simon SI. Leukocyte function antigen-1, kindlin-3 and calcium flux orchestrate neutrophil recruitment during inflammation. *J Immunol.* 2012; 189:5954-5964
- [3] Abram CL and Lowell CA. The ins and outs of leukocyte integrin signaling. *Annu Rev Immunol.* 2009; 27: 339-362
- [4] Dixit N, Yamayoshi I, Nazarian A, Simon SI. Migrational guidance of neutrophils is mechanotransduced via high-affinity LFA-1 and calcium flux. *J Immunol.* 2011; 187: 472-481
- [5] Schaff UY, Dixit N, Procyk E, Yamayoshi I, Tse T, Simon SI. Orai1 regulates intracellular calcium, arrest, and shape polarization during neutrophil recruitment in shear flow. *Blood.* 2010; 115: 657-666
- [6] Haumer M, Amighi J, Exner M, Mlekusch W, Sabeti S, Schlager O, et al. Association of neutrophils and future cardiovascular events in patients with peripheral artery disease. *J Vascular Surgery.* 2005; 41(4): 610-617
- [7] Amulic B, Cazalet C, Hayes GL, Metzler KD, Zychlinsky A. Neutrophil function: from mechanisms to disease. *Ann Rev of Immunol.* 2012; 30: 459-489
- [8] Chase SD, Magnani JL, Simon SI. E-selectin ligands as mechanosensitive receptors on neutrophils in health and disease. *Ann Biomed Eng.* 2012; 40(4): 849-59
- [9] Mitroulis I, Alexaki VI, Kourtzelis I, Ziogas A, Hajishengallis G, Chavakis T. Leukocyte integrins: role in leukocyte recruitment and as therapeutic targets in inflammatory disease. *Pharmacol Ther.* 2015; 147: 123-35
- [10] Saito Y. Roles of atrial natriuretic peptide and its therapeutic use. *Journal of Cardiology.* 2010; 56: 262-270
- [11] Mizuno Y, Yasue H, Oshima S, Yoshimura M, Ogawa H, Morita E, et al. Effects of angiotensin-converting enzyme inhibitor on plasma B-type natriuretic peptide levels in patients with acute myocardial infarction. *J Card Fail.* 1997; 3: 287-293
- [12] Biselli R, Farrace S, De Simone C, Fattorossi A. Potentiation of human polymorphonuclear leukocyte activation by atrial natriuretic peptide. Inhibitory effect of carnitine congeners. *Inflammation.* 1996; 20: 33-42

- 1 [13] Suwa M, Seino Y, Nomachi Y, Matsuki S, Funahashi K. Multicenter prospective
2 investigation on efficacy and safety of carperitide for acute heart failure in the ‘real world’ of
3 therapy. *Circ J*. 2005; 69(3): 283-90
4
- 5 [14] Hayashi M, Tsutamoto T, Wada A, Maeda K, Mabuchi N, Tstsui T, et al. Intravenous atrial
6 natriuretic peptide prevents left ventricular remodeling in patients with first anterior acute
7 myocardial infarction. *J Am Coll Cardiol*. 2001; 37(7): 1820-6
- 8 [15] Vollmar AM. The role of atrial natriuretic peptide in the immune system. *Peptides*. 2005;
9 26(6):1086-94.
10
- 11 [16] Nojiri T, Hosoda H, Tokudome T, Miura K, Ishikane S, Okumura M, et al. Atrial natriuretic
12 peptide prevents cancer metastasis through vascular endothelial cells. *Proc Natl Acad Sci USA*
13 2015; 112(13): 4086-4091
14
- 15 [17] Kierner AK, Weber NC, Fürst R, Bildner N, Kulhanek-Heinze S, Vollmar AM. Inhibition of
16 p38 MAPK activation via induction of MKP-1: atrial natriuretic peptide reduces TNF-alpha-
17 induced actin polymerization and endothelial permeability. *Circ Res*. 2002; 90(8):874-81.
18
- 19 [18] Tian X1, Tian Y, Gawlak G, Sarich N, Wu T, Birukova AA. Control of vascular
20 permeability by atrial natriuretic peptide via a GEF-H1-dependent mechanism. *J Biol Chem*.
21 2014; 289(8):5168-83.
22
- 23 [19] Mtairag el M, Houard X, Rais S, Pasquier C, Oudghiri M, Jacob MP, et al. Pharmacological
24 potentiation of natriuretic peptide limits polymorphonuclear neutrophil-vascular cell interactions.
25 *Arterioscler Thromb Vasc Biol*. 2002;22(11):1824-31.
26
- 27 [20] Kierner AK, Vollmar AM. Autocrine regulation of inducible nitric oxide synthase in
28 macrophages by atrial natriuretic peptide. *J Biol Chem*. 1998; 273:13444-51
29
- 30 [21] De Vito P. Atrial natriuretic peptide: An old hormone or a new cytokine. *Peptides*. 2014; 58:
31 108-16
32
- 33 [22] Baldini PM, De Vito P, Martino A, Fraziano M, Grimaldi C, Luly P et. al. Differential
34 sensitivity of human monocytes and macrophages to ANP: a role of intracellular pH and reactive
35 oxygen species production through the phospholipase involvement. *J Leukoc Biol*. 2003; 73(4):
36 502-10
37
- 38 [23] Kuhn M. Endothelial actions of atrial and B-type natriuretic peptides. *Br J Pharmacol*. 2012;
39 166(2): 522-31
40
- 41 [24] Damiano ER, Westheider J, Tözeren A, Ley K. Variation in the velocity, deformation, and
42 adhesion energy density of leukocytes rolling within venules. *Circ Res*. 1996; 79: 1122-30
43
- 44 [25] Firrell JC, Lipowsky HH. Leukocyte margination and deformation in mesenteric venules of
45 rat. *Am J Physiol*. 1989; 256: 1667-74

- 1
2 [26] Sundd P, Gutierrez E, Pospieszalska MK, Zhang H, Groisman A, Ley K. Quantitative
3 dynamic footprinting microscopy reveals mechanisms of neutrophil rolling. *Nat Methods*. 2010;
4 7(10): 821-824
5
6 [27] Kim MH, Curry FR, Simon SI. Dynamics of neutrophil extravasation and vascular
7 permeability are uncoupled during aseptic cutaneous wounding. *Am J Physiol Cell Physiol*.
8 2009; 296(4):C848-56.
9
10 [28] Evans E, Yeung A. Apparent viscosity and cortical tension of blood granulocytes
11 determined by micropipette aspiration. *Biophys J*. 1989; 13(9): 941-954
12
13 [29] Tran-Son-Tay R, Needham D, Yeung A, Hochmuth RM. Time dependent recovery of
14 passive neutrophils after the large deformation. *Biophys J*. 1991; 60(4): 856-866
15
16 [30] Tran-Son-Tay R, Kirk TF 3rd, Zhelev DV, Hochmuth RM. Numerical simulation of the flow
17 of highly viscous drops down a tapered tube. *J Biomech Eng*. 1994; 116(2): 172-7
18
19 [31] Needham D, Hochmuth RM. Rapid flow of passive neutrophils into 4 microns pipet and
20 measurement of cytoplasmic viscosity. *J Biomech Eng*. 1990; 112(3): 269-276
21
22 [32] Needham D, Hochmuth RM. A sensitive measure of surface stress in the resting neutrophil.
23 *Biophys J*. 1992; 61(6): 1664-1670
24
25 [33] Potter LR. Natriuretic peptide metabolism, clearance and degradation. *FEBS J*. 2011;
26 278(11): 1808-17
27
28 [34] Curry FE, Jiang Y, Kim MH, Clark JF, Adamson RH, Simon SI. The Role of Atrial
29 Natriuretic Peptide to Attenuate Inflammation (Abstract 672.4) *FASEB Journal* 2014
30
31 [35] Zhang H, Schaff UY, Green CE, Simon SI. Impaired integrin-dependent function in
32 Wiskott-Aldrich syndrome protein-deficient murine and human neutrophils. *Immunit*. 2006;
33 25(2):285-295.
34
35
36 [36] Herant M, Heinrich V, Dembo M. Mechanics of neutrophil phagocytosis: behavior of the
37 cortical tension. *J Cell Sci*. 2005; 118(9):1789-97
38
39 [37] Dixit N, Kim MH, Rossaint J, Yamayoshi I, Zarbock A, Simon SI. Leukocyte function
40 antigen-1, kindlin-3, and calcium flux orchestrate neutrophil recruitment during inflammation. *J*
41 *Immunol*. 2012; 189(12): 5954-64
42
43 [38] Nomura F, Kurobe N, Mori Y, Hikita A, Kawai M, Suwa M, et al. Multicenter prospective
44 investigation on efficacy, safety of carperitide as a first-line drug for acute heart failure
45 syndrome with preserved blood pressure: COMPASS: carperitide effects observed through
46 monitoring dyspnea in acute decompensated heart failure study. *Circ J*. 2008; 72:1777-1786.

- 1
2 [39] Brandt RR, Wright RS, Redfield MM, Burnett JC Jr. Atrial natriuretic peptide in heart
3 failure. *J Am Coll Cardiol.* 1993; 22: 86A-92A
4
- 5 [40] Hirano K. The roles of proteinase-activated receptors in the vascular physiologu and
6 pathophysiology. *ATVB.* 2007; 27(1):27-36
- 7 [41] Vergnolle N, Derian CK, D'Andrea MR, Steinhoff M, and Andrade-Gordon P.
8 Characterization of thrombin-induced leukocyte rolling and adherence: a potential
9 proinflammatory role for proeinase-activated receptor-4. 2002; 169(3): 1467-73
- 10 [42] Futosi K, Fodor S, Mocsai A. Reprint of neutrophil cell surface receptors and their
11 intracellular signal transduction pathways. *Int Immunopharmacol.* 2013; 17)4_: 1185-97
- 12 [43] Firrell JC, Lipowsky HH. Leukocyte margination and deformation in mesenteric venules of
13 rat. *Am J Physiol.* 1989; 256: 1667-74
14
- 15 [44] Rocheleau AD, Sumagin R, Sarelius IH, King MR. Simulation and analysis of tethering
16 behavior of neutrophils with pseudopods. *PloS One.* 2015; 10(6): e0128378
17
- 18 [45] Dembo M, Torney DC, Saxman K, Hammer D. The reaction-limited kinetics of membrane-
19 to-surface adhesion and detachment. *Proc R Soc Lond B Biol Sci.* 1988; 234(1274): 55-83
20
- 21 [46] Ward MD, Dembo M, Hammer DA. Kinetics of cell detachment: peeling of discrete
22 receptor clusters. *Biophysical Journal.* 1994; 67: 2522-2534
23
- 24 [47] Sundd P, Pospieszalska MK, Ley K. Neutrophil rolling at high shear: flattening, catch bond
25 behavior, tethers and slings. *Mol Immunol.* 2013; 55(1): 59-69
26
- 27 [48] Spiering D, Hodgson L. Dynamics of the Rho-family GTPases in actin regulation and
28 motility. *Cel Adh Migr.* 2011. 5(2): 170-80
29
- 30 [49] Liu X, Wang X, Tin H, Chen H. Deformation mechanism of leukocyte adhering to vascular
31 surface under steady shear flow. *Sci China C Life Sci.* 2004; 47(2): 165-74
32
- 33 [50] Dinauer MC. Regulation of neutrophil function by Rac GTPases. *Curr Opin Hematol.* 2003;
34 10(1):8-15
35
- 36 [51] Lee CW, Vitriol EA, Shim S, Wise AL, Velayutham RP, Zheng JQ. Dynamic localization
37 of G-actin during membrane protrusion in neuronal motility. *Curr Biol.* 2013; 23(12): 1046-56
38
- 39 [52] Arcaro A. The small GTP-binding protein Rac promotes the dissociation of gelsolin from
40 the actin filaments in neutrophils. *J Biol Chem.* 1998; 273(2): 805-813
41
- 42 [53] Lőrincz ÁM, Szarvas G, Smith SM, Ligeti E. Role of Rac GTPase activating protein in
43 regulation of NADPH oxidase in human neutrophils. *Free Radic Biol Med.* 2014; 68:65-71

- 1
2 [54] Sundd P, Pospieszalska MK, Cheung LS, Konstantopoulos K, Ley K. Biomechanics of
3 leukocyte rolling. *Biorheology*. 2011; 48: 1-35
4
- 5 [55] Pawar P, Jadhav S, Eggleton CD, Konstantopoulos K. Roles of cell and microvillus
6 deformation and receptor-ligand binding kinetics in cell rolling. *Am J Physiol Heart Circ*
7 *Physiol*. 2008; 295: H1439-H1450
8
- 9 [56] Marshal BT, Long M, Piper JW, Yago T, McEver RP, Zhu C. Direct observation of catch
10 bonds involving cell-adhesion molecules. *Nature*. 2003; 423: 190-193
11
- 12 [57] Damiano ER, Westheider J, Tözeren A, Ley K. Variation in the velocity, deformation, and
13 adhesion energy density of leukocytes rolling within venules. *Circ Res*. 1996; 79: 1122-30
14
- 15 [58] Cao J, Donell B, Deaver DR, Lawrence MB, Dong C. In vitro side-view imaging technique
16 and analysis of human T-leukenic cell adhesion to ICAM-1 in shear flow. *Microvasc Res*. 1998;
17 55(2): 124-37
18

1 **6 Tables**

2 **Table 1. Membrane tension and viscosity of PMN obtained from micropipette experiments.**

3 A cortical shell-liquid core rheological model was applied to compute the material constants.
4 Viscosity was approximated using the ratio of cortical tension to viscosity from the
5 recovery/relaxation measurements and the observed cortical tension from the micropipette
6 aspiration experiments.

σ (mN/m)	σ/η ($\mu\text{m/s}$)	η (Pa·s)	Study
0.021 ± 0.013	0.117	~179	Untreated
0.023 ± 0.007	0.071	~324	10 nM ANP
0.035	N.D	210 ± 100	[26]
N.D.	0.17	151.7 ± 39.8	[27]
0.035	0.13 – 0.26	N.D	[28]
N.D.	N.D	135 ± 54	[32]
0.024 ± 0.003	N.D	N.D	[33]
0.018	0.132 ± 0.043	136	[34]

7

8

1 **7 Figure Legends**

2 **Figure 1. ANP down-regulates neutrophil recruitment on inflamed endothelium**
3 **independent of adhesion receptor expression. (A)** A full thickness skin wound was performed
4 in Lys-M-EGFP mice and at 24 hours PMN accumulation was quantified over a 60 minute
5 interval in response to Thrombin stimulation (5 U/mL) in presence and absence of perfusion of
6 ANP (50ng/kg/min). Representative images of PMN fluorescence intensity in the wound bed are
7 depicted for each treatment condition. **(B)** PMN accumulation in wound over 60 min relative to
8 saline control is plotted as rate of change of PMN fluorescence (FI/min; significant attenuation
9 versus ANP by ANOVA with Tukey multiple comparison test, n=6 mice, # depicts p<0.05). **(C)**
10 Endothelial adhesion receptor expression was assessed on IL-1 β (0.2 ng/ml) stimulated HUVEC
11 as a function of ANP concentration. The relative increase in receptor expression normalized to
12 the baseline level on non-stimulated endothelium is plotted (n=3, mean \pm SEM). No significance
13 was found between IL-1 β stimulated versus ANP.

14

1 **Figure 2. ANP inhibits PMN capture and shear resistant independent of cellular adhesion**
2 **receptor activation. (A)** PMN rolling, arrest, and transendothelial migration (TEM) quantified
3 at 2 dynes/cm² on IL-1 β inflamed HUVEC was measured from video record as mean \pm SEM
4 number per four FOVs and analyzed from 3 separate microfluidic flow channels. n=3 separate
5 donors. *** signifies significance between ANP and vehicle control p<.005, ** signifies
6 significance between ANP and vehicle control p<.01, and * signifies significance between ANP
7 and control p<.05 **(B)** PMN (1x10⁶ cells/mL) were pretreated with 1-10 nM ANP and
8 continuously perfused over recombinant ICAM-1 + E-selectin substrates in a microfluidic flow
9 chamber. The number of PMN remaining adherent relative to the number at 2 min. under 2
10 dynes/cm². Shear was incremented every 30 seconds as depicted up to 40 dynes/cm². The
11 numbers of PMN remaining in the presence or absence of ANP at the indicated dose were
12 recorded from 3 separate donors. Nearly all PMN treated with vehicle control convert to shear
13 resistant arrest, while ANP treated PMN formed long membrane tethers that abruptly ruptured
14 upon detachment. Line plots are polynomial regression fits to the data points. **(C)** PMN tether
15 formation for PMN arrested at 2 dynes/cm² and ramped to 10 dynes/cm². Images of tether length
16 defined as point of contact with substrate to the center of the cell are shown just before cell
17 detachment. PMN tether length significantly increased at the low and high dose of ANP
18 treatment compared with vehicle control (p<.05, n=3). **(D)** Isolated PMNs (1x10⁶ cells/mL) were
19 analyzed by flow cytometry for expression of β_2 -integrin and L-selectin adhesion receptors
20 following 15 min. stimulation with IL-8 (10 nM) after pretreatment with the indicated dose of
21 ANP for 30 minutes prior to measurement. ANP did not alter the up-regulation of β_2 -integrin or
22 the shedding of L-selectin when compared to untreated control (n=3). PMN F-actin was
23 measured using Phalloidin with and without IL-8 stimulation after simultaneous fixing and
24 permeabilization. Data shows replicates for n=3 donors with no significant effect of ANP
25 observed.

26

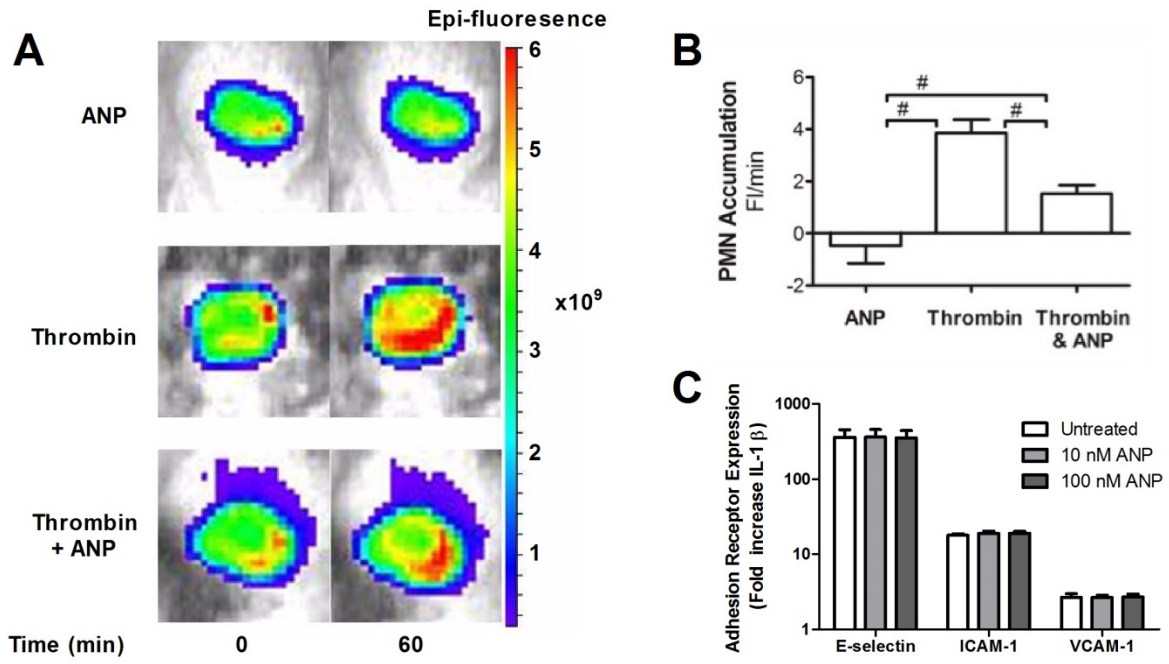
1 **Figure 3. Rheological analysis of PMN cortical tension and viscosity.** Untreated and 10 nM
2 ANP treated PMN were suspended in HEPES buffered saline with 10% autologous serum to
3 maintain unactivated and non-adherent state. **(A)** PMN were aspirated into the micropipette and
4 held for 10 sec. prior to expulsion into the chamber. Kinetics of recovery back to spherical state
5 (e.g. defined as length to width ratio of 1.1) was recorded and depicted in representative images.
6 ANP treated PMN recovered ~30% slower than vehicle control. **(B)** Time constant for recovery
7 was fit to a viscoelastic model yielding an estimate of cortical tension/viscosity [26,27].
8 Histograms of vehicle control versus ANP were Gaussian fit as depicted. Untreated PMNs (red
9 line) versus 10 nM ANP (black) show a significant left shift in the tension/viscosity ratio due to
10 ANP treatment (n=50 PMN per condition analyzed from n=4 separate donors) **(C)** PMN were
11 partially aspirated into a micropipette while internal pressure was slowly increased and plotted
12 versus protrusion length of hemispherical cap as depicted in images. Laplace's law was used to
13 estimate cortical tension and correlate it with a fractional increase in surface area from resting
14 spherical state (see Methods). A linear regression was used to compute resting cortical tension in
15 vehicle control (0.021 ± 0.013) and 10 nM ANP treated cells (0.023 ± 0.007) (n=50 PMN
16 analyzed from 4 separate experiments. No significance found between control and ANP
17 treatment.
18
19

1 **Figure 4. Adhesive contact area and β_2 -integrin-ICAM-1 bond formation during PMN**
2 **arrest and shear strengthening.** Vehicle control versus 10 nM ANP treated PMN (2×10^6
3 cells/mL) were perfused in the microfluidic flow chamber at 1 dyne/cm² on a substrate of
4 recombinant E-selectin and ICAM-1. **(A)** TIRF images of PMN arrested for 30 sec before shear
5 was incremented up to 20 dynes/cm² at which time shear stress was returned to 0 dynes/cm²
6 revealing PMN remained deformed on substrate. **(B)** PMN membrane adhesive contact area was
7 quantified using image analysis of the membrane dye DiO over time course of shear ramp for
8 vehicle control versus 10 nM ANP (n=3 separate donors, representative of 30 PMN per
9 treatment) **(C)** Membrane contact area versus shear stress for vehicle control and ANP treatment.
10 Fractional increase is plotted versus 2 dyne/cm² for 30 sec. for each condition, respectively (n=30
11 PMN per condition, n=3 separate donors). **(D)** High affinity CD18 quantified from TIRF images
12 of mAb24-AF488 fluorescence within area of adhesive contact on PMN from previous shear
13 ramp figure (no significance found using student t test, n=24 cells over 3 donors). **(E)** CD18
14 focal adhesion clusters per PMN contact area. Representative images depict individual clusters,
15 Significance difference for the 10 nM ANP condition (p<.05, n=24 cells over 3 donors).
16

1 **Figure 5. Schematic depicting PMN deformation and integrin bond formation under shear**
2 **flow.** PMN form stable CD18/ICAM-1 bonds that support cell arrest. The top macroscopic view
3 depicts a PMN deforming from a spherical to a tethered and elongated geometry relative to the
4 direction of flow (θ_b). The hydrodynamic shear force (F_s) translates membrane tension (τ) into a
5 ~~resistive-disruptive~~ bond force (F_b) that act on bond clusters within the adhesive contact region.
6 Top view depicts the increase in adhesive contact area allowing for the formation of CD18 bond
7 clusters. With ANP treatment there is less deformation, which maintains a larger (θ_b) and greater
8 translation of membrane tension (τ) to fewer bond clusters and thus a relative higher breakage
9 force (F_b) on fewer bond clusters.

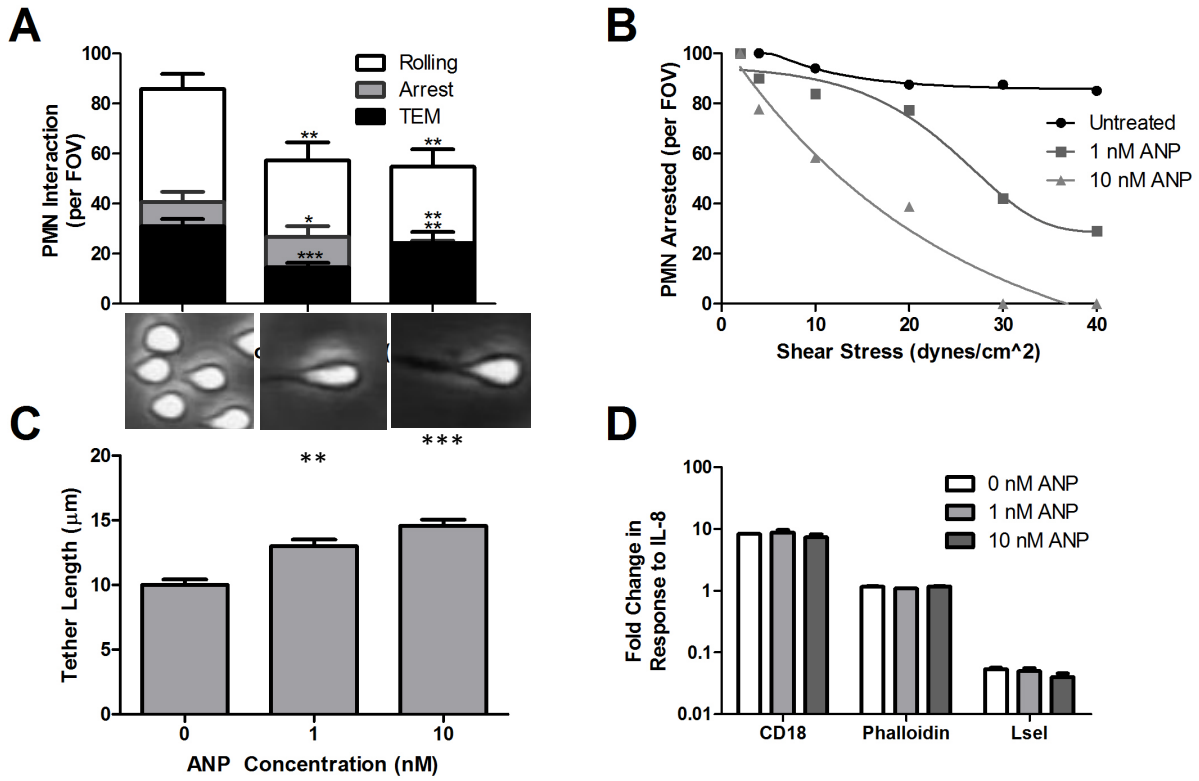
10

1 **Figure 1**



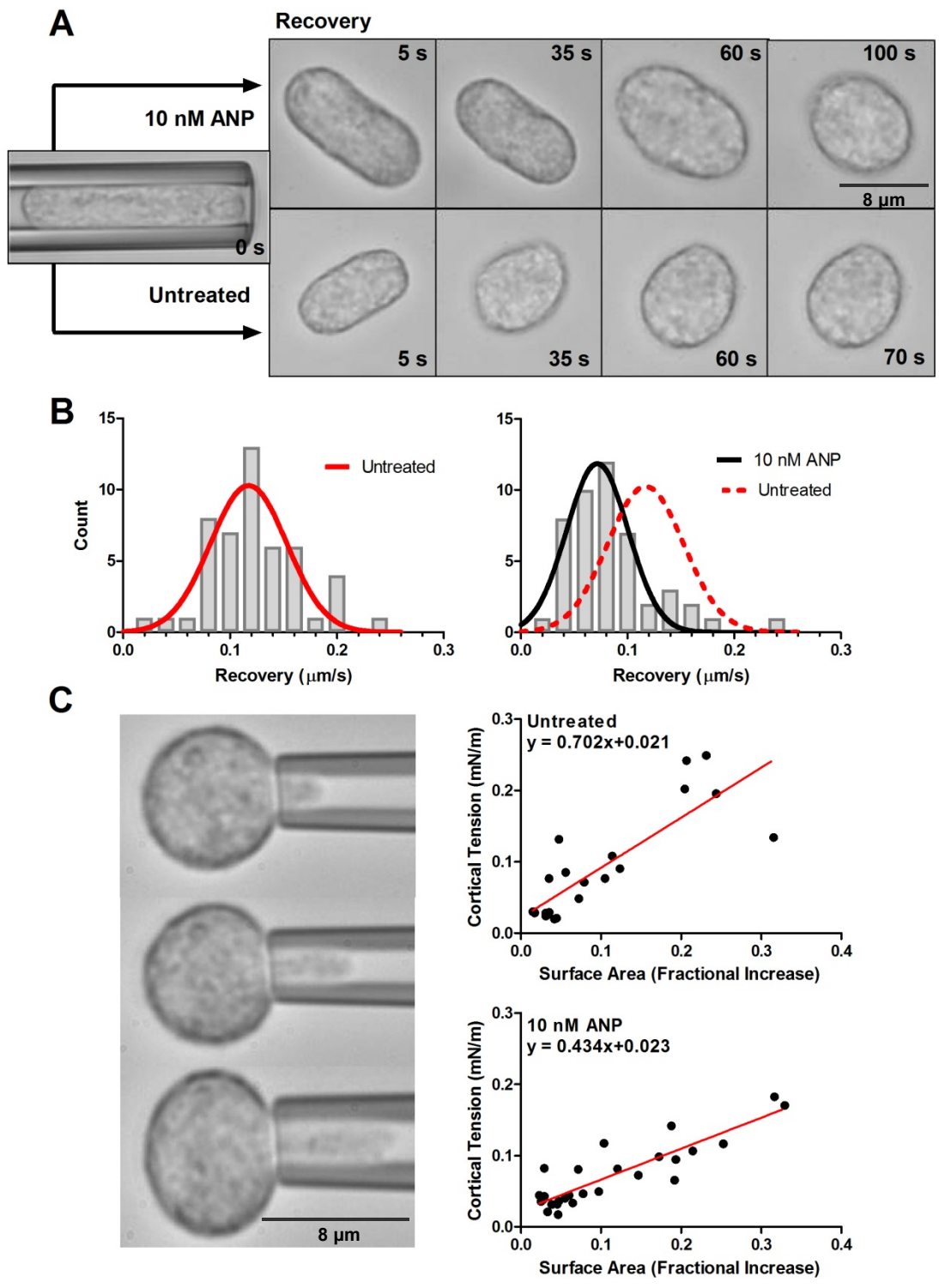
2

1 **Figure 2**



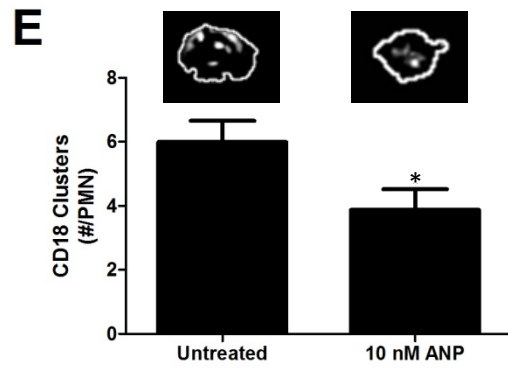
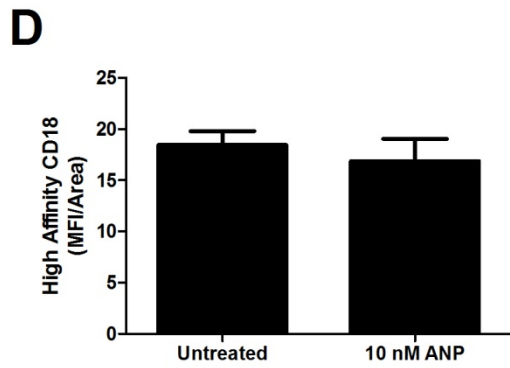
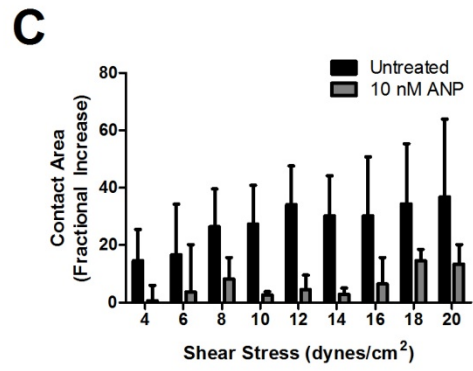
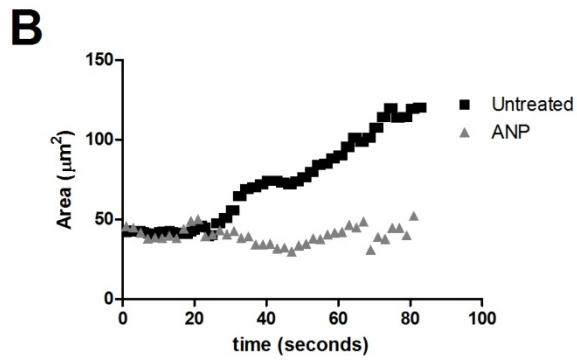
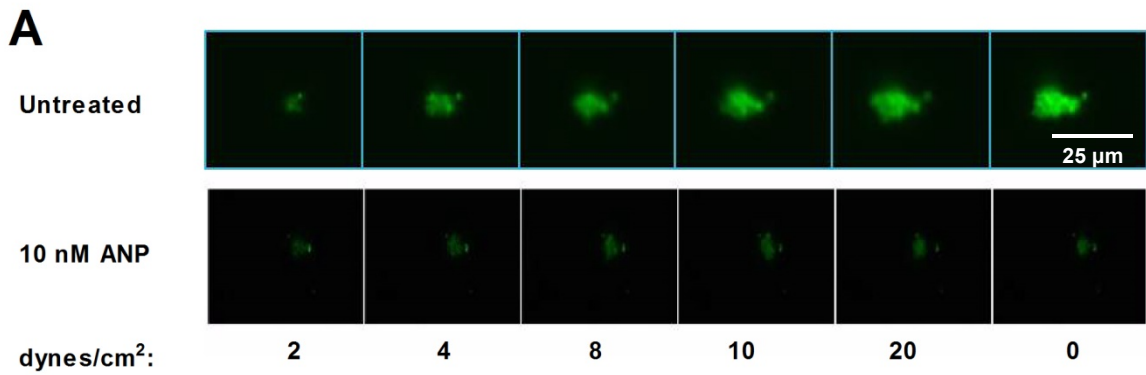
2
3

1 **Figure 3**



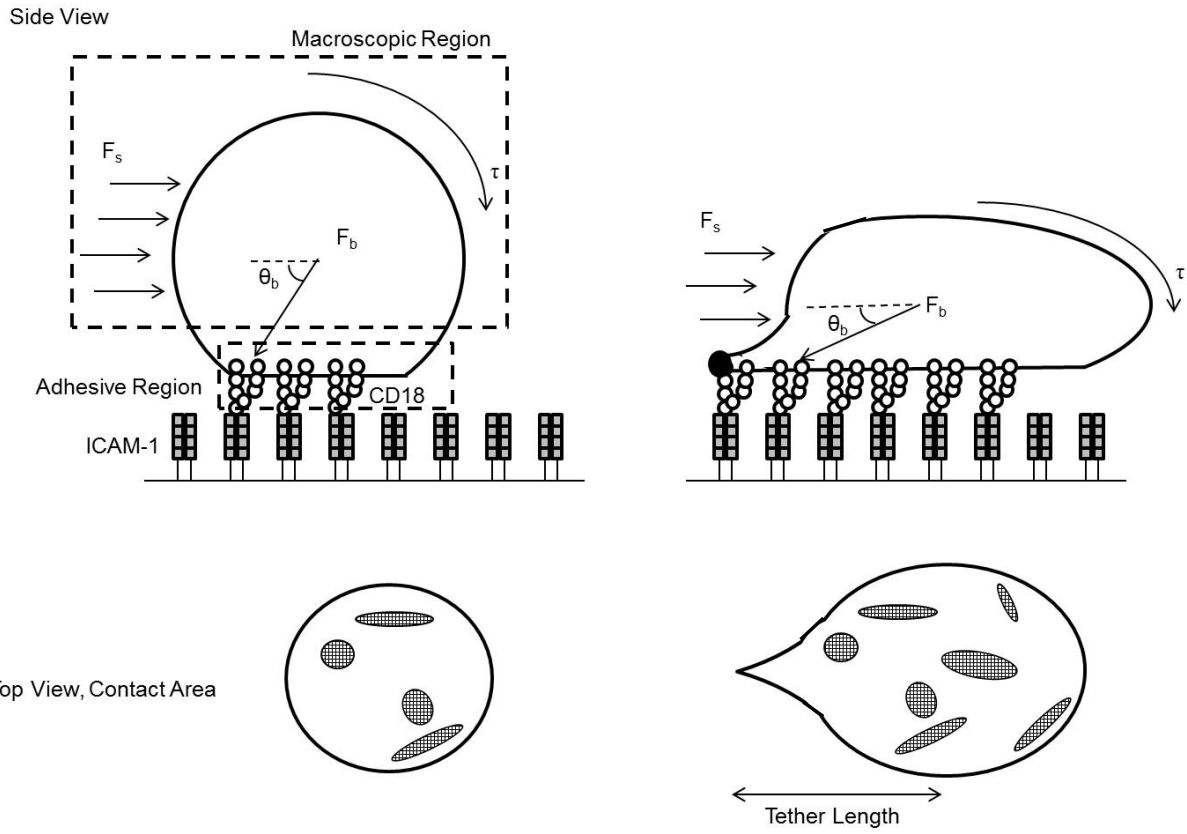
2

1 **Figure 4**



2

1 **Figure 5**



2

3